Geophysical Research Letters

RESEARCH LETTER
10.1029/2024GL108649

Stratospheric Chlorine Processing After the Unprecedented Hunga Tonga Eruption

Jun Zhang[1], Peidong Wang[2], Douglas Kinnison[1], Susan Solomon[2], Jian Guan[2], Kane Stone[2], and Yunqian Zhu[3,4]

[1]Atmospheric Chemistry Observations & Modeling Laboratory, NSF National Center for Atmospheric Research, Boulder, CO, USA, [2]Department of Earth, Atmospheric, and Planetary Sciences, Massachusetts Institute of Technology, Cambridge, MA, USA, [3]Cooperative Institute for Research in Environmental Sciences, University of Colorado Boulder, Boulder, CO, USA, [4]Chemical Sciences Laboratory, National Oceanic and Atmospheric Administration, Boulder, CO, USA

Key Points:

- Analysis using both model and satellites suggest a significant role of chemical processing in the observed HCl reduction at 20 km
- Analysis of gas- and heterogeneous-phase reactions indicates that heterogeneous chemistry is the main driver for the chemical loss of HCl
- The dominant heterogeneous loss for HCl is via HOBr + HCl, with HCl + OH also significant due to enhanced OH from heterogeneous chemistry

Supporting Information:

Supporting Information may be found in the online version of this article.

Correspondence to:

J. Zhang,
jzhan166@ucar.edu

Citation:

Zhang, J., Wang, P., Kinnison, D., Solomon, S., Guan, J., Stone, K., & Zhu, Y. (2024). Stratospheric chlorine processing after the unprecedented Hunga Tonga eruption. *Geophysical Research Letters*, *51*, e2024GL108649. https://doi.org/10.1029/2024GL108649

Received 5 FEB 2024
Accepted 17 AUG 2024

Abstract Following the Hunga Tonga–Hunga Ha'apai (HTHH) eruption in January 2022, significant reductions in stratospheric hydrochloric acid (HCl) were observed in the Southern Hemisphere mid-latitudes during the latter half of 2022, suggesting potential chlorine activation. The objective of this study is to comprehensively understand the loss of HCl in the aftermath of HTHH. Satellite measurements and a global chemistry-climate model are employed for the analysis. We find strong agreement of 2022 anomalies between the modeled and the measured data. The observed tracer-tracer relations between nitrous oxide (N_2O) and HCl indicate a significant role of chemical processing in the observed HCl reduction, especially during the austral winter of 2022. Further examining the roles of chlorine gas-phase and heterogeneous chemistry, we find that heterogeneous chemistry emerges as the primary driver for the chemical loss of HCl, and the reaction between hypobromous acid (HOBr) and HCl on sulfate aerosols is the dominant loss process.

Plain Language Summary After the eruption of the Hunga Tonga–Hunga Ha'apai (HTHH) volcano in January 2022, there was a substantial decrease in stratospheric hydrochloric acid (HCl) in the Southern Hemisphere mid-latitudes in the latter part of 2022. This decrease suggests that a chemical reaction involving chlorine processing might have happened. This study aims to comprehensively understand the significant loss of HCl following the HTHH eruption, utilizing satellite measurements and a global chemistry-climate model for analysis. The anomalies in 2022 show remarkable agreement between the modeled and measured data. By comparing the levels of HCl with another gas called nitrous oxide (N_2O), we discover that a lot of the HCl loss was due to chemical reactions, especially during the Southern Hemisphere winter. Upon further investigation into the role of chlorine gas-phase and heterogeneous chemistry, heterogeneous chemistry emerges as a primary driver for the chemical loss of HCl. The reaction between hypobromous acid (HOBr) and HCl on sulfate aerosols is identified as the dominant loss process.

1. Introduction

The January 2022 Hunga Tonga–Hunga Ha'apai (HTHH) eruption (20.5°S, 175.4°W) was an unprecedented modern era underwater volcanic event. The eruption injected about 150 Tg of water (H_2O) along with a moderate amount of sulfur dioxide (SO_2) into the stratosphere (e.g., Carn et al., 2022; Millán et al., 2022; Taha et al., 2022). Satellite observations and model simulations found significant ozone decreases in the lower stratosphere at Southern Hemisphere (SH) mid-latitudes in 2022 after the eruption (Santee et al., 2023; Wilmouth et al., 2023). In particular, record low ozone relative to the climatology (2004–2021) in the SH austral winter between 30 and 50 hPa was observed in the mid-latitudes (Zhang, Wang, et al., 2024). While there is evidence for some dynamical contributions to the ozone variations observed in 2022 (Wang et al., 2023), anomalous reductions in mid-latitude chlorine (Cl) reservoir species hydrochloric acid (HCl) along with enhancements in reactive chlorine monoxide (ClO) (Santee et al., 2023; Wilmouth et al., 2023), suggest that Cl chemistry likely contributed to the record low ozone abundances.

It is well-known that the SO_2 emission from volcanic eruptions can enhance aerosol surface areas and heterogeneous chemistry (e.g., Hofmann & Solomon, 1989; Solomon, 1999). As the volcanic aerosols of HTHH spread, measurements from the Microwave Limb Sounder (MLS) and Optical Spectrograph and InfraRed Imager System reported large reductions in concentrations of stratospheric nitrogen oxide (NO_x), via hydrolysis of dinitrogen pentoxide (N_2O_5) on aerosols (Santee et al., 2023; Zhang, Wang, et al., 2024). In response, the concentration of

ClO increases as less NO_x is available to convert ClO into reservoir species chlorine nitrate ($ClONO_2$). But N_2O_5 hydrolysis does not affect HCl to any significant degree. Santee et al. (2023) highlighted the role of dynamics in influencing HCl mixing ratio anomalies, particularly during the latter part of 2022. Nevertheless, tracer-tracer analysis by Wilmouth et al. (2023) shows deviations in MLS-observed HCl and N_2O relationship, suggesting that chemical losses of HCl cannot be ignored. The underlying reasons behind the chemical loss of HCl are the subject of this study.

There are several possible pathways for the HCl chemical loss. A major mechanism driving HCl loss is the heterogeneous reaction $HCl + ClONO_2 \rightarrow Cl_2 + HNO_3$ on and within particles, leading to the production of highly reactive chlorine (Solomon et al., 2015). This heterogenous chlorine reaction is highly temperature dependent and is only effective on the surfaces of typical stratospheric aerosols and polar stratospheric clouds at temperatures below 195 K (Hanson et al., 1994, 1996; Kawa et al., 1997; Shi et al., 2001; Solomon et al., 2015). Mid-latitude temperatures are generally too warm (>200K) for this heterogeneous reaction to take place. Following the HTHH eruption, stratospheric H_2O injection has the potential to elevate the threshold temperature for chlorine activation, enabling chlorine processing in mid-latitudes (Anderson et al., 2012; Kirk-Davidoff et al., 1999; Solomon et al., 1999). Additionally, heterogeneous bromine reactions on stratospheric sulfate aerosols have been examined by a number of groups (e.g., Abbatt, 1995; Hanson & Ravishankara, 1995; Slusser et al., 1997; Tie & Brasseur, 1996). These studies indicate that with high aerosol surface areas $HOBr + HCl \rightarrow BrCl + H_2O$ could represent a significant loss process for HCl at mid-latitudes. Later measurements reported by Waschewsky and Abbatt (1999) and Hanson (2003) further suggest that under warm stratospheric conditions (205–220 K), HCl loss via reaction with HOBr could become significant. The nearly temperature-independent hydrolysis of bromine nitrate ($BrONO_2$) can serve as a significant source of HOBr under elevated aerosol loadings. Recent studies have also emphasized the ability of organic aerosols from wildfires to activate chlorine in the mid-latitude lower stratosphere (Bernath et al., 2022; Santee et al., 2023; Solomon et al., 2022, 2023). Thus, it is important to distinguish between the chemistry occurring on volcanic aerosols compared to that on wildfire and other organic-aerosols at mid-latitudes.

Further, the conversion of HCl to reactive chlorine via the gas-phase reaction $HCl + OH \rightarrow Cl + H_2O$ may be accelerated by elevated OH levels in the aftermath of the HTHH eruption. The massive injection of H_2O leads to a direct and rapid increase in stratospheric OH abundances (Wilmouth et al., 2023; Zhu et al., 2022). In addition, photolysis of the gas-phase HNO_3, HOCl and HOBr produced from the hydrolysis of N_2O_5, $ClONO_2$, and $BrONO_2$ is a source of reactive hydrogen, HO_x ($OH + HO_2$). The reduction in NO_x concentration also contributes to an increase in HO_x by impeding the rate of the reaction between NO_2 and OH.

This study aims to discern whether chlorine activation primarily occurs through gas-phase or heterogeneous chemistry in the wake of HTHH, and determine the processes that are responsible for the chemical loss of HCl. This work will not quantify ozone changes; rather, it will be exclusively focused on the chlorine chemistry in the SH mid-latitudes during the 2022 austral winter. The ozone impact and ozone chemistry has been discussed in Zhang, Wang, et al. (2024).

2. Data and Method

2.1. Satellite Data

Data sets are from the Atmospheric Chemistry Experiment-Fourier Transform Spectrometer (ACE- FTS), MLS and the Ozone Mapping and Profiler Suite Limb Profiler (OMPS-LP). Level 2 satellite data from ACE-FTS version 5.2 are employed for H_2O, N_2O and HCl (Boone et al., 2023). Additionally, daily level 3 satellite data from MLS version 5.0 are used for N_2O and HCl (Livesey et al., 2020). Both data sets span from 2007 to 2022 to match with the model simulation period. We exclude 2020–2021 because of the Australian new year's wildfire in late 2019/early 2020 (Bernath et al., 2022; Santee et al., 2023; Solomon et al., 2022, 2023; Strahan et al., 2022). Anomalies for N_2O and HCl in 2022 (Figure 1) are calculated as deviations from the mean of the 2007–2019 climatological background. Livesey et al. (2021) pointed out the long-term trend of MLS N_2O is suffering from a ∼3–4% per decade drift in the lower stratosphere. Here, we detrend MLS daily data to allow an interannual comparison. Aerosol extinction data are from the University of Saskatchewan OMPS-LP product (Bourassa et al., 2023). These data, obtained via tomographic inversion, offer height-resolved aerosol extinction measurements at 745 nm, with a vertical resolution of 1–2 km.

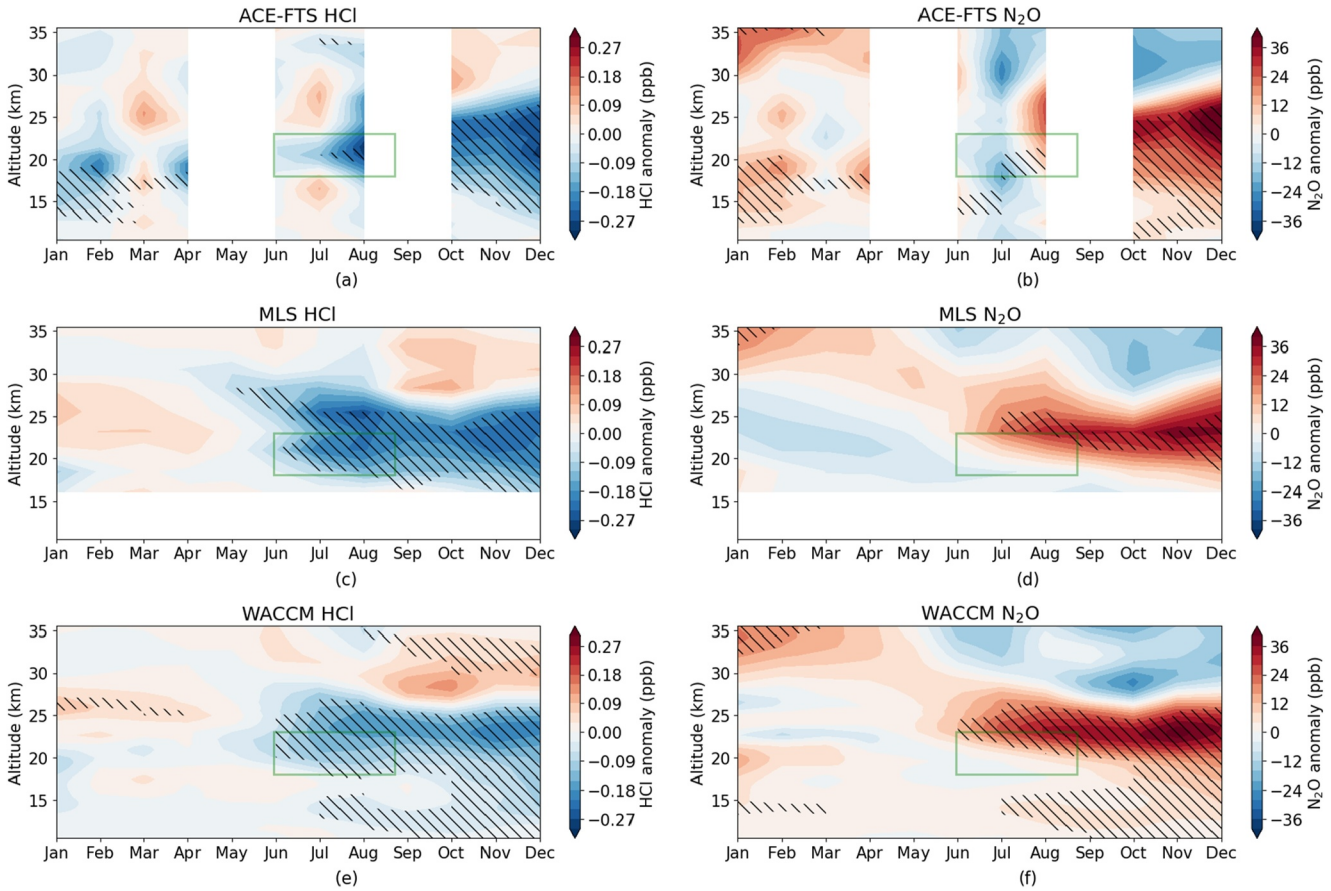

Figure 1. Calculated 2022 HCl anomaly in ppbv (panel a,c,e) and N_2O anomaly in ppbv (panel b,d,f) relative to climatology (2007–2019) from ACE-FTS, MLS, and WACCM in the SH mid-latitudes (30–55°S). Hatched regions indicate where the 2022 anomalies are outside the range of all variability during 2007–2019.

2.2. Community Earth System Model Version 2 (CESM2)/Whole Atmosphere Community Climate Model (WACCM)

The numerical experiments were conducted using CESM2/WACCM6, a state-of-the-art chemistry-climate model that spans from the Earth's surface to approximately 140 km. The model incorporates a comprehensive representation of troposphere-stratosphere-mesosphere-lower-thermosphere (TSMLT) chemistry, with detailed descriptions available in Gettelman et al. (2019). WACCM6 features a prognostic stratospheric aerosol module (Mills et al., 2016) and has been extensively employed to investigate the impact of volcanic aerosols on heterogeneous processes and their impact on ozone loss (e.g., Mills et al., 2017; Stone et al., 2017; Zambri et al., 2019). Table S1 in Supporting Information S1 lists the references for key stratospheric heterogeneous processes on volcanic aerosols used in WACCM.

The simulations here are characterized by a horizontal resolution of 0.9° latitude × 1.25° longitude. The model includes 110 vertical levels, with a vertical resolution of approximately 500m in the upper troposphere and lower stratosphere. WACCM6 is operated in a specified dynamics configuration, where temperatures and horizontal winds are relaxed to the Modern-Era Retrospective analysis for Research and Applications Version 2 (MERRA-2) reanalysis (Gelaro et al., 2017) using a relaxation timescale of 12 hr (Davis et al., 2022). This configuration spans from 2007 until the end of 2022, initialized with conditions from a long historical simulation (Gettelman et al., 2019). The model setup incorporates major stratospheric volcanic injections from 2007 to 2021. Beginning in January 2022, two distinct cases are conducted: the volcano case with SO_2 and H_2O injection from the HTHH eruption, and the control case with no emissions from the HTHH eruption. The disparity between these two nudged simulations provides insights into the chemistry-related changes following the HTHH eruption. This study assumes the emissions are 150 Tg H_2O and 0.6 Tg SO_2 on 15 January 2022, from approximately 20 to 35 km altitude. The injection profiles of H_2O and SO_2 are similar to Zhu et al. (2022), however, with an adjustment of

SO_2 injection. The SO_2 injection estimate ranges from 0.4 to 1 Tg (e.g., Li et al., 2023; Millan et al., 2022; Sellitto et al., 2023) from different sources and approaches. Here an SO_2 injection of 0.6 Tg is utilized, leading to aerosol extinction that exhibits strong agreement with the OMPS-LP observations, especially during the 2022 Austral winter (Figure S1 in Supporting Information S1).

2.3. Tracer-Tracer Method

Exploring the correlation among chemical species, commonly known as "tracer–tracer" analysis, is a means to dissect the interactions between dynamical and chemical processes (e.g., Griffin et al., 2019; Proffitt et al., 1990). We construct a "no-chemistry" baseline from the linear fit between N_2O and HCl over January to March data, since no or little heterogeneous chemistry normally occurs in these 3 months given the warm conditions. N_2O is used to clarify the influence of dynamics in shaping the distribution of trace gasses. The foundation of this analysis lies in the expectation that dynamical transport should impact both N_2O and HCl in a similar manner. The deviations of HCl from this "no-chemistry" baseline are defined as Δ HCl, indicating the changes in HCl that are due to chemical processes. A detailed discussion on this method can be found in Wang et al. (2023).

In this analysis, N_2O serves as an inactive tracer for calculating Δ HCl, given its availability in both ACE-FTS and MLS observations. The distinct long-term trends of N_2O and HCl resulting from anthropogenic emissions could introduce a bias in the tracer-tracer correlation. Furthermore, the drifting issue associated with MLS N_2O adds complexity to the long-term trends. To address this, Δ HCl for each year is computed based on the "no-chemistry" baseline established in that specific year. This approach prevents long-term trends in N_2O and HCl from affecting the calculations.

3. Results and Discussions

3.1. Chemical Signal of HCl Loss at Mid-latitudes (30–55°S)

The 2022 anomalies are computed as deviations from the climatological mean, shown in Figure 1. We linearly detrend both satellite observations and model simulations using data from 2007 to 2019 to accommodate the long-term trends in N_2O and HCl as well as additional instrumental drift in MLS N_2O. The climatology encompasses various phases of the Quasi-Biennial Oscillation (QBO). Therefore, the derived stratospheric anomalies in HCl and N_2O reflect both the influence of the 2022 QBO phase and the forced changes after the HTHH eruption, including both dynamical and chemical impacts. Notably, in much of the lower stratosphere, the vertical and meridional gradients of N_2O exhibit an opposite pattern to HCl. As a result, N_2O is generally anticorrelated with HCl in the lower stratosphere. The hatched regions on the plot denote areas where the 2022 anomalies fall outside the range of all variability during the period 2007–2019. Specifically, for N_2O and HCl, the hatches indicate that the 2022 value represents the maximum and minimum, respectively, compared to the climatological data. The WACCM N_2O anomaly is consistent with observations (Figures 1b–1f), suggesting that the dynamical transport tracers are well represented in WACCM.

The WACCM HCl anomaly in 2022 closely aligns with ACE-FTS and MLS relative to the climatology. Differences between ACE-FTS and MLS can arise from various reasons (e.g., data coverage). The onset of the negative anomaly in HCl is evident from May, corresponding to the arrival of substantial aerosols from the HTHH eruption in this region (Santee et al., 2023). During the winter months of June, July, and August (JJA), ACE-FTS, MLS, and WACCM consistently display the lowest HCl levels compared to all years included in the climatology (hatched in Figures 1a–1e), consistent with the large negative HCl anomaly in the winter reported in Wilmouth et al. (2023). In the latter part of the year, specifically between 17 and 27 km, both model and observations exhibit a substantial negative anomaly in HCl. Despite the potential for chemical processing in this region, any signal of chemical processing is overshadowed by significant countervailing positive anomalies in N_2O, indicating the predominant influence of transport effects. However, in the key altitudes of approximately 18–22 km during JJA that we focus on here (green boxes in Figure 1), the large HCl anomaly is not accompanied by a similarly large N_2O anomaly. This discrepancy suggests that dynamics alone cannot account for the low HCl levels in that region, and chemical processing is likely taking place. The subsequent analysis will focus on this specific region during the SH mid-latitudes JJA.

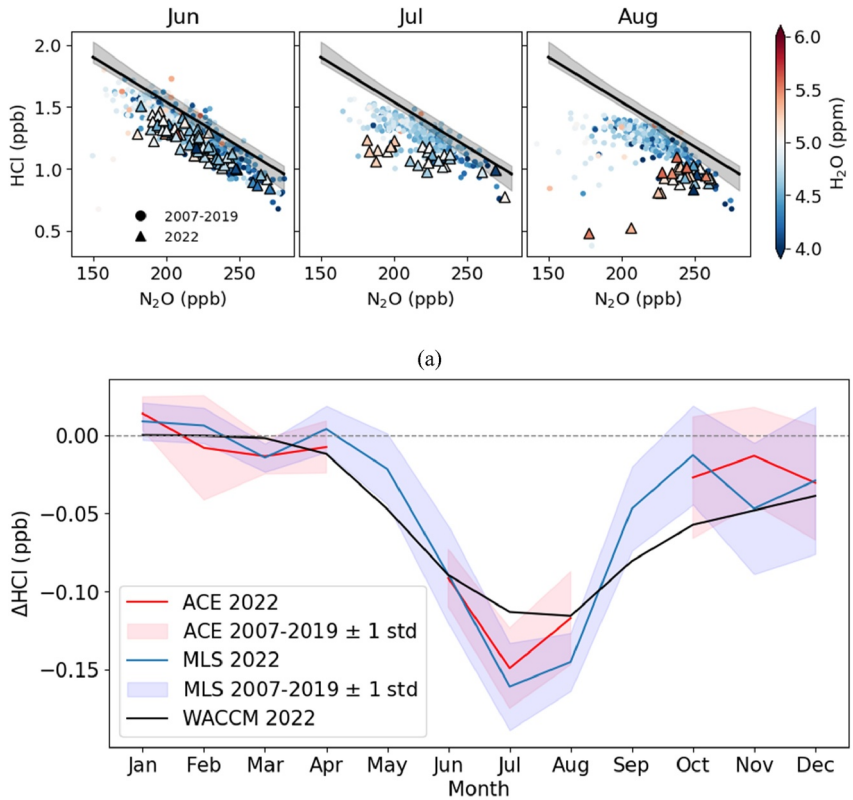

Figure 2. (a) Tracer–tracer correlation between ACE-FTS-measured N_2O (*x*-axis) and HCl (*y*-axis), color-coded by H_2O concentration. Each dot represents a single measurement at 20.5 km over 30 to 55°S. The thick black lines represent the no-chemistry baseline, from the linear fit over January–March 2022 data points. The shaded regions indicate a conservative full range of baseline variability bounded by the maximum and minimum baselines constructed by data in individual years from 2007 to 2019. (b) Calculated ΔHCl from ACE-FTS, MLS and WACCM in 2022 averaging all points over 30 to 55°S, with the seasonal cycle removed. ACE-FTS and MLS ΔHCl is calculated from departures from the baseline in (a), representing the change in HCl due to anomalous chemical processes in 2022. The blue and red shaded regions indicate ±1 standard deviation range for MLS and ACE-FTS in each month from 2007 to 2019.

3.2. Significant Stratospheric Chlorine Activation

Figure 2a demonstrates the method of retrieving satellite data and performing the tracer-tracer analysis. It depicts the tracer-tracer relationship of ACE-FTS N_2O and HCl in June, July and August at 20.5 km over 30 to 55°S, color-coded by H_2O concentration. ACE-FTS doesn't have observations in May and September 2022 over this latitude range. The thick black lines in Figure 2a represent the "no-chemistry" baseline in 2022, and the shaded area encompasses a conservative full range of baseline variability, bounded by the maximum and minimum baselines between 2007 and 2019. Deviations from correlation observed in HCl suggest the presence of chemical processes, as described in Wang et al. (2023). The intensity of chemical processes becomes more pronounced with greater deviations of HCl from the baseline. Tracer-tracer plots further confirm the strong chemical processing that occurs in June and intensifies in July and August in 2022 compared to 2007 to 2019 (triangles in Figure 2a). It is notable that deviations in HCl from their respective "no-chemistry" baseline occur in June to August from 2007 to 2019 (round points in Figure 2a), as a small amount chlorine activation happens every year in these months with a seasonal cycle.

Figure 2b displays the derived ΔHCl resulting from chemical processes from MLS, ACE-FTS, and WACCM in 2022. ACE-FTS and MLS ΔHCl is calculated by the deviations from the baseline, with the seasonal cycle removed. Shaded regions in blue and red represent the range of ±1 standard deviation (std) for MLS and ACE-FTS ΔHCl, respectively, for each month from 2007 to 2019. The patterns of derived ΔHCl from observations

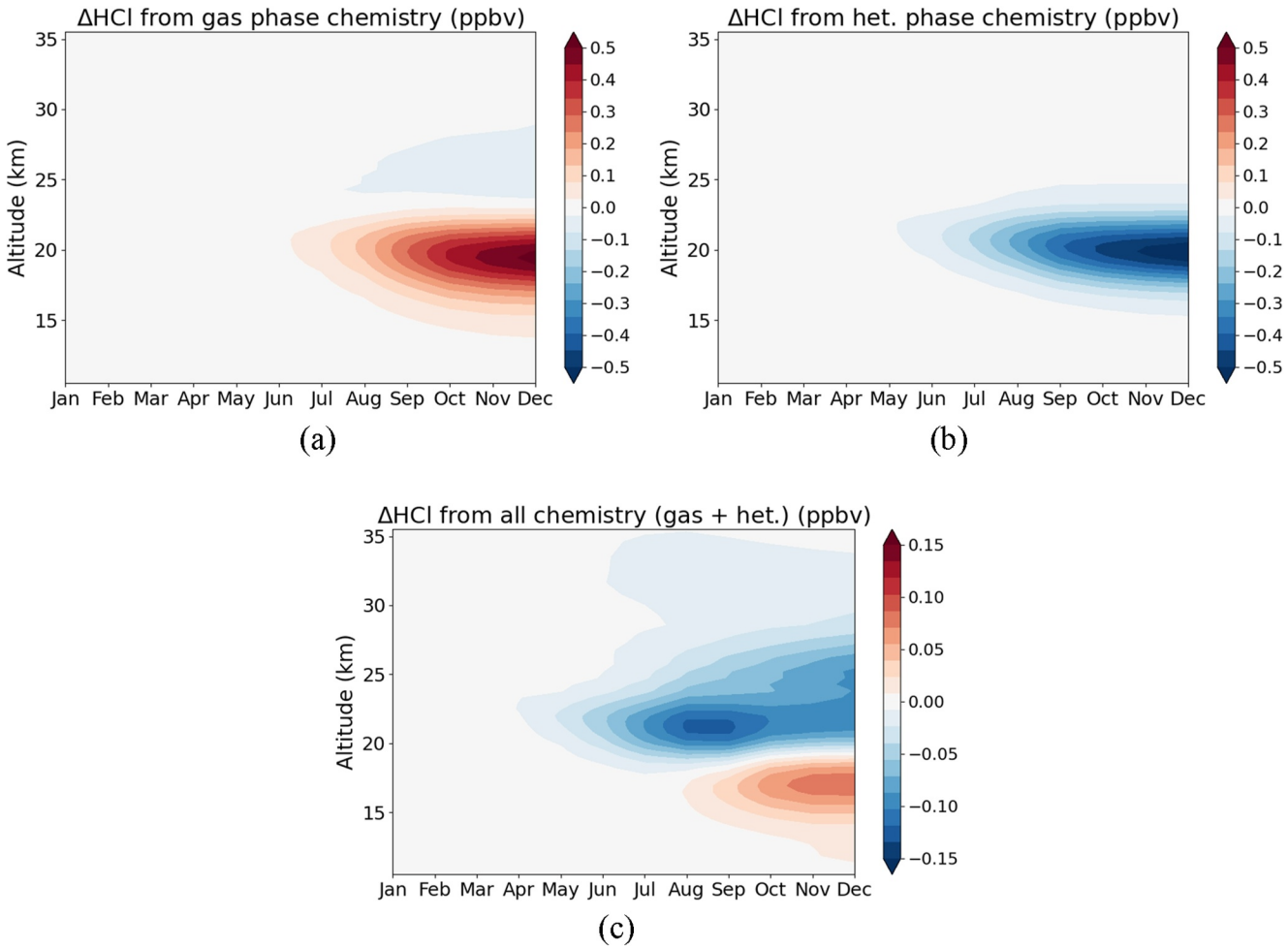

Figure 3. WACCM calculated ΔHCl (ppbv) from the volcano minus the control case for (a) gas-phase chemistry only, (b) heterogeneous chemistry only and (c) the sum of all gas and heterogeneous chemistry over 30 to 55°S. Note that panels c has different color bar ranges from panels a and (b).

closely resemble those calculated by WACCM from the two nudged simulations (volcano minus control). Notably, the largest chemical induced HCl reduction occurs in the SH winter. Figure 2b further indicates that tracer-tracer analysis can effectively be employed to derive ΔHCl due to chemical processes using MLS and ACE-FTS data, and the results are comparable with those from the chemistry climate model. The differences between WACCM, ACE-FTS and MLS are within the uncertainty range ±1 std (blue and red shaded region in Figure 2b).

3.3. Role of Gas and Heterogenous Phase Chemistry in Chlorine Activation

To understand the chemical processes that give rise to the ΔHCl in Figure 2 following the HTHH eruption, a thorough model examination is conducted. Figure 3 illustrates the changes in gas-phase and heterogeneous-phase chemistry, along with the cumulative changes of all chemistry. The ΔHCl is calculated from the volcano case compared to the control case. Gas-phase chemistry (Figure 3a) results in an increase in HCl below 23 km over the 30 to 55°S, accompanied by a decrease from 23 to 30 km attributed to the HCl + OH reaction. Heterogeneous chemistry (Figure 3b) induces HCl depletion from 15 to 25 km. Considering both gas and heterogeneous chemistry (Figure 3c), the ΔHCl exhibits a net reduction above 19 km from April to December, with the maximum reduction occurring in the winter, consistent with Figure 2. There is an HCl increase below 18 km (Figure 3c), attributable to enhanced gas-phase reactions, particularly Cl + CH_4 and ClO + OH (discussed below).

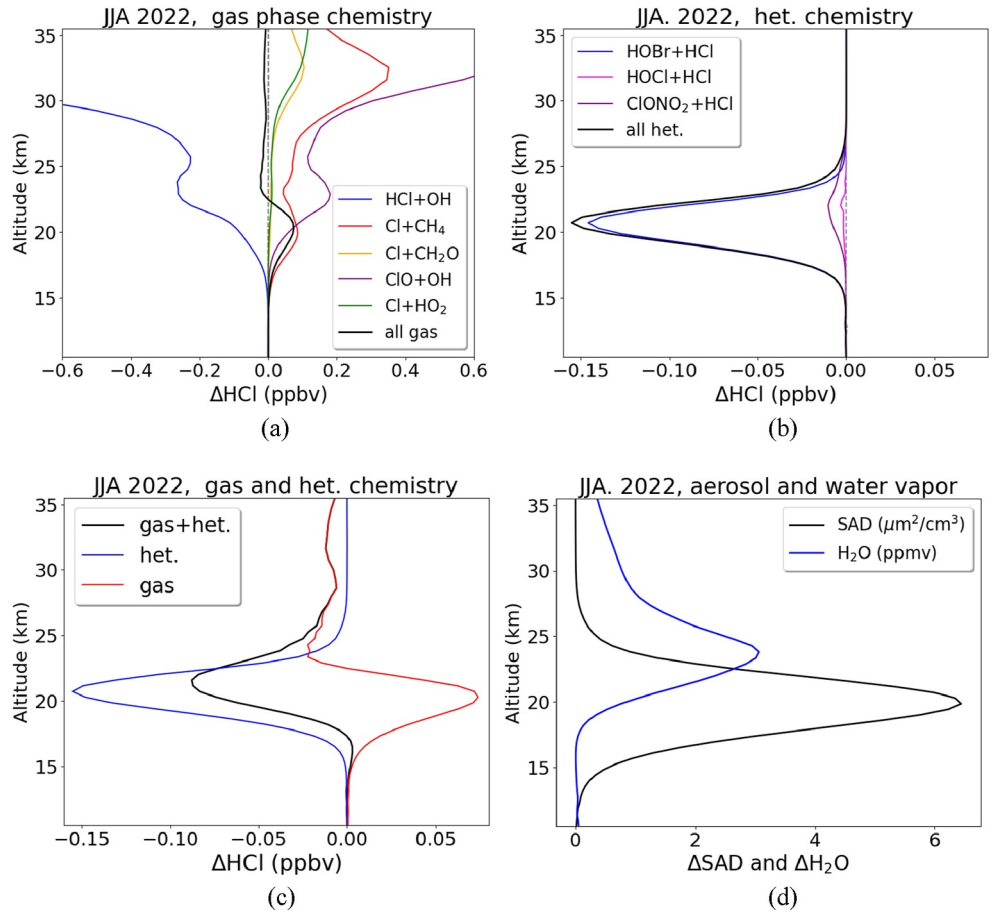

Figure 4. ΔHCl (in ppbv) contribution from individual reactions for (a) gas chemistry, (b) het. chemistry and (c) the sum of all chemistry averaged over JJA in 2022 over 30 to 55°S. ΔHCl is calculated from the volcano minus control case. (d) The modeled aerosol surface area density in $\mu m^2/cm^3$ and water in ppmv. Note that panels a has different a scale range from panels b and (c).

Perturbations in individual reactions are investigated following the HTHH eruption, with a particular focus during JJA. The reactions with important contributions to the ΔHCl are plotted in Figure 4 with different colors. The rest of the reactions only affect less than 1% of ΔHCl, thus are not shown here. A full list of HCl reactions examined can be found in Table S2 in Supporting Information S1. The "all gas" black line in Figure 4a adds up all the gas reactions, not just the gas terms plotted in the figures, and same for the "all het" black line in Figure 4b, which sums up all the heterogeneous reactions. In the realm of gas-phase chemistry (Figure 4a), the reaction between HCl and elevated OH acts as the dominant significant sink for HCl from the simulated perturbation due to HTHH. However, this loss is entirely compensated for by the heightened gas-phase production, particularly Cl + CH_4 and ClO + OH. Among heterogeneous reactions (Figure 4b), the primary sink for HCl is the reaction between HOBr and HCl on sulfate aerosols between 18 and 22 km, with $ClONO_2$+HCl contributing as well, albeit with a much smaller magnitude. This result is mainly attributed to volcanic aerosols providing additional surface area density (SAD) for heterogeneous chemistry at these altitudes (Figure 4d). Here we conclude that, during the SH wintertime, the HCl abundance reduction from 18 to 22 km in the mid-latitudes is mainly attributed to heterogeneous chemistry rather than gas-phase chemistry (Figure 4c).

The injection of volcanic water and aerosols from the HTHH eruption perturbs atmospheric conditions (e.g., surface area density, aerosol radius and H_2SO_4 content), which further impact the reactive probability of heterogeneous reactions (Santee et al., 2023; Zhu et al., 2023). Comparative analysis between the volcano case and the control case reveals enhanced reaction probabilities for all examined heterogeneous reactions in the volcano scenario, as shown in Figure S2 in Supporting Information S1. The conditions used to derive these reaction probabilities are listed in Table S3 in Supporting Information S1. Laboratory studies (e.g., Hanson, 2003;

Waschewsky & Abbatt, 1999) have demonstrated the highly efficient hydrolysis of $BrONO_2$ in sulfuric acid solutions. Reaction probabilities of approximately 0.8 were documented for the uptake of $BrONO_2$ onto sulfuric acid solutions with H_2SO_4 content ranging from 40 to 70 weight percentage. Compared to other heterogeneous processes, hydrolysis of $BrONO_2$ is relatively temperature-insensitive and can take place rapidly at various stratospheric conditions, making its influence important and widespread. The product HOBr undergoes heterogeneous reaction with HCl, providing an additional pathway to chlorine activation. Under temperatures in the mid-latitudes (>200K), the enhancement in the rate of the HOBr + HCl reactions after the HTHH eruption plays a dominant role in HCl depletion among all the heterogeneous processes. Additional sensitivity studies indicate that the gas-phase reaction OH + HCl also contributes to the HCl loss. However, the OH concentrations below approximately 22 km are largely enhanced by heterogeneous chemistry, particularly through the photolysis of HOBr and HOCl produced via heterogeneous $ClONO_2$ and $BrOBO_2$ hydrolysis (detail in Text S1 in Supporting Information S1).

3.4. HCl Activation by HOBr + HCl in Stratospheric Sulfuric Acid Aerosol

Both $BrONO_2$ and HCl are taken up in sulfate aerosols. In modeling the reaction HOBr + HCl, either the reaction probability for HCl (γHCl) or for HOBr (γHOBr) is used. In WACCM6 γHOBr is employed for calculations. Under identical conditions, γHOBr is significantly larger than γHCl as shown in Figure S6 in Supporting Information S1. To assess the impact of using either γHOBr or γHCl in calculating the HOBr + HCl reaction rate, we conducted several tests in a box model (described in Text S2 in Supporting Information S1). Our findings indicate that the rates of the HOBr + HCl reaction remain remarkably similar regardless of which γ is used (Figure S7 in Supporting Information S1). Thus, using γHOBr instead of γHCl does not significantly affect the loss of HCl. The reason is that this heterogeneous reaction is not rate-limiting under the relevant stratospheric conditions. Instead, the heterogeneous reaction proceeds very quickly, with the formation of $BrONO_2$ and, consequently, HOBr being the rate-limiting step.

The increased water concentration at mid-latitudes leads to a reduction in sulfuric acid content in the volcano case. This decelerates the second-order rate coefficient (k^{II}), which exhibits a strong dependency on acidity. In WACCM we utilize the kinetics recommendations from Hanson (2003) to compute the γHOBr of HOBr + HCl. According to Hanson, k^{II} approaches the diffusion-limited value at approximately 70% wt., resulting in the efficacy of HOBr + HCl decreasing precipitously for acid contents greater than 70 wt.%. In the volcano case, the reduced sulfuric acid content leads to the diffusion limit being reached and a subsequent decrease in the reaction probability of HOBr + HCl at warmer temperatures compared to the control case.

The latest JPL-19 assessment does not recommend kinetics parameters for HOBr + HCl. It cites Waschewsky and Abbatt (1999) (WA99) and Hanson (2003), noting that the differences between their findings are not fully understood and that further laboratory work is needed. In addition to the Hanson study, we also assessed the kinetics proposed by WA99 to determine the γ for HOBr + HCl, as illustrated in Figure S3b in Supporting Information S1. Their study indicates that k^{II} reaches the diffusion limit at lower acidity levels, resulting in a decline in the reaction probability of HOBr + HCl at cooler temperatures compared to Hanson. Discrepancies in these results may arise from uncertainties in the solubility of HCl, upon which k^{II} is quadratically dependent. Furthermore, variations in the reported HOBr solubility between the two studies (a factor of 3–10) significantly impact the diffusion-limited k^{II} value.

We conducted further experiments by implementing different γ of HOBr + HCl, derived from the aforementioned studies, into our box model to assess their impact on reaction rates and the resulting ΔHCl (Figure S7 in Supporting Information S1). Our findings indicate that the rates of heterogeneous HOBr + HCl reactions are largely consistent between the two studies until mid-August. However, the rates derived from WA99 begin to decline from mid-August onward. This decline corresponds to WA99 reaching the diffusion-limited value at cooler temperatures compared to Hanson. This indeed results in smaller ΔHCl compared to Hanson's value. We acknowledge that our base case using Hanson (2003) can be regarded as an upper limit of the derived ΔHCl, while WA99 can be considered a lower limit.

4. Summary

In summary, we have examined the mid-latitudes HCl reduction in the SH winter following the eruption of HTHH using satellite data and global chemistry-climate model. Our analysis indicates a significant role for

heterogeneous chemical processing in the observed HCl reduction. The results confirm that the tracer-tracer method provides a good estimate of the chemical impacts distinct from dynamics. The derived chemical HCl change is consistent among ACE-FTS, MLS and WACCM. Further delving into WACCM's detailed chemistry, we examine individual chlorine gas-phase and heterogeneous reactions. We find that despite a substantial increase in the reaction of HCl with elevated OH in the SH winter, this loss is entirely compensated for by heightened gas-phase production from Cl + CH_4 and ClO + OH. Heterogeneous chemistry emerges as a primary driver for the chemical loss of HCl, with the reaction between HOBr and HCl on sulfate aerosols identified as the most crucial process. Our study provides useful information for understanding volcanic impacts on stratospheric chemistry, particularly their detailed breakdown among gas-phase and heterogeneous reactions at mid-latitudes.

Data Availability Statement

CESM2/WACCM6 (described in Gettelman et al., 2019) is an open-source community model and is available at https://www.cesm.ucar.edu/models/cesm2. CESM2/WACCM6 was developed with support primarily from the National Science Foundation. Figures in this study are plotted using an open-source software Python (https://www.python.org/downloads/). The atmospheric modeling data set and the box model (Text S1 in Supporting Information S1) used in the analysis is published (Zhang, Wang, et al., 2024).

Acknowledgments
Jun Zhang is supported by the NSF via NCAR's Advanced Study Program Postdoctoral Fellowship. Douglas Kinnison is partially supported by NASA Grant 80NSSC19K0952. Peidong Wang, Susan Solomon and Jian Guan gratefully acknowledge support by NSF-AGS [2316980]. NCAR's Community Earth System Model project is supported primarily by the National Science Foundation. This material is based upon work supported by the NSF National Center for Atmospheric Research, which is a major facility sponsored by the U.S. National Science Foundation under Cooperative Agreement No. 1852977. Computing and data storage resources, including the Cheyenne supercomputer (doi:10.5065/D6RX99HX), were provided by the Computational and Information Systems Laboratory (CISL) at NCAR. This project received funding from NOAA's Earth Radiation Budget (ERB) Initiative (CPO #03-01-07-001). Yuqian Zhu is supported in part by NOAA cooperative agreements NA17OAR4320101 and NA22OAR4320151. We thank the valuable feedbacks from Dr. David Wilmouth from Harvard University. The outputs from CESM2/WACCM6 and the box model used in the analysis is published and can be obtained from https://doi.org/10.5065/j6yg-a009.

References

Abbatt, J. P. (1995). Interactions of HBr, HCl, and HOBr with supercooled sulfuric acid solutions of stratospheric composition. *Journal of Geophysical Research*, *100*(D7), 14009–14017. https://doi.org/10.1029/95jd01367

Anderson, J. G., Wilmouth, D. M., Smith, J. B., & Sayres, D. S. (2012). UV dosage levels in summer: Increased risk of ozone loss from convectively injected water vapor. *Science*, *337*(6096), 835–839. https://doi.org/10.1126/science.1222978

Bernath, P., Boone, C., & Crouse, J. (2022). Wildfire smoke destroys stratospheric ozone. *Science*, *375*(6586), 1292–1295. https://doi.org/10.1126/science.abm5611

Boone, C. D., Bernath, P. F., & Lecours, M. (2023). Version 5 retrievals for ACE-FTS and ACE-imagers. *Journal of Quantitative Spectroscopy and Radiative Transfer*, *310*, 108749. https://doi.org/10.1016/j.jqsrt.2023.108749

Bourassa, A. E., Zawada, D. J., Rieger, L. A., Warnock, T. W., Toohey, M., & Degenstein, D. A. (2023). Tomographic retrievals of Hunga Tonga-Hunga Ha'apai volcanic aerosol. *Geophysical Research Letters*, *50*(3), e2022GL101978. https://doi.org/10.1029/2022GL101978

Carn, S. A., Krotkov, N. A., Fisher, B. L., & Li, C. (2022). Out of the blue: Volcanic SO2 emissions during the 2021–2022 eruptions of Hunga Tonga—Hunga Ha'apai (Tonga). *Frontiers in Earth Science*, *10*, 976962. https://doi.org/10.3389/feart.2022.976962

Davis, N. A., Callaghan, P., Simpson, I. R., & Tilmes, S. (2022). Specified dynamics scheme impacts on wave-mean flow dynamics, convection, and tracer transport in CESM2 (WACCM6). *Atmospheric Chemistry and Physics*, *22*(1), 197–214. https://doi.org/10.5194/acp-22-197-2022

Gelaro, R., McCarty, W., Suárez, M. J., Todling, R., Molod, A., Takacs, L., et al. (2017). The modern-era retrospective analysis for research and applications, version 2 (MERRA-2). *Journal of Climate*, *30*(14), 5419–5454. https://doi.org/10.1175/JCLI-D-16-0758.1

Gettelman, A., Mills, M. J., Kinnison, D. E., Garcia, R. R., Smith, A. K., Marsh, D. R., et al. (2019). The whole atmosphere community climate model version 6 (WACCM6). *Journal of Geophysical Research: Atmospheres*, *124*(23), 12380–12403. https://doi.org/10.1029/2019JD030943

Griffin, D., Walker, K. A., Wohltmann, I., Dhomse, S. S., Rex, M., Chipperfield, M. P., et al. (2019). Stratospheric ozone loss in the Arctic winters between 2005 and 2013 derived with ACE-FTS measurements. *Atmospheric Chemistry and Physics*, *19*(1), 577–601. https://doi.org/10.5194/acp-19-577-2019

Hanson, D. R. (2003). Reactivity of BrONO2 and HOBr on sulfuric acid solutions at low temperatures. *Journal of Geophysical Research*, *108*(D8). https://doi.org/10.1029/2002jd002519

Hanson, D. R., & Ravishankara, A. R. (1995). Heterogeneous chemistry of bromine species in sulfuric acid under stratospheric conditions. *Geophysical Research Letters*, *22*(4), 385–388. https://doi.org/10.1029/94gl03379

Hanson, D. R., Ravishankara, A. R., & Lovejoy, E. R. (1996). Reaction of BrONO2 with H2O on submicron sulfuric acid aerosol and the implications for the lower stratosphere. *Journal of Geophysical Research*, *101*(D4), 9063–9069. https://doi.org/10.1029/96jd00347

Hanson, D. R., Ravishankara, A. R., & Solomon, S. (1994). Heterogeneous reactions in sulfuric acid aerosols: A framework for model calculations. *Journal of Geophysical Research*, *99*(D2), 3615–3629. https://doi.org/10.1029/93jd02932

Hofmann, D. J., & Solomon, S. (1989). Ozone destruction through heterogeneous chemistry following the eruption of El Chichon. *Journal of Geophysical Research*, *94*(D4), 5029–5041. https://doi.org/10.1029/JD094iD04p05029

Kawa, S. R., Newman, P. A., Lait, L. R., Schoeberl, M. R., Stimpfle, R. M., Kohn, D. W., et al. (1997). Activation of chlorine in sulfate aerosol as inferred from aircraft observations. *Journal of Geophysical Research*, *102*(D3), 3921–3933. https://doi.org/10.1029/96jd01992

Kirk-Davidoff, D. B., Hintsa, E. J., Anderson, J. G., & Keith, D. W. (1999). The effect of climate change on ozone depletion through changes in stratospheric water vapour. *Nature*, *402*(6760), 399–401. https://doi.org/10.1038/46521

Li, Z., Bi, J., Hu, Z., Ma, J., & Li, B. (2023). Regional transportation and influence of atmospheric aerosols triggered by Tonga volcanic eruption. *Environmental Pollution*, *325*, 121429. https://doi.org/10.1016/j.envpol.2023.121429

Livesey, N. J., Read, W. G., Froidevaux, L., Lambert, A., Santee, M. L., Schwartz, M. J., et al. (2021). Investigation and amelioration of long-term instrumental drifts in water vapor and nitrous oxide measurements from the Aura Microwave Limb Sounder (MLS) and their implications for studies of variability and trends. *Atmospheric Chemistry and Physics*, *21*(20), 15409–15430. https://doi.org/10.5194/acp-21-15409-2021

Livesey, N. J., Read, W. G., Wagner, P. A., Froidevaux, L., Santee, M. L., & Schwartz, M. J. (2020). Version 5.0 x level 2 and 3 data quality and description document (tech. Rep. No. JPL D-105336 rev. A). *Jet Propulsion Laboratory*.

Millan, L., Santee, M. L., Lambert, A., Livesey, N. J., Werner, F., Schwartz, M. J., et al. (2022). The Hunga Tonga-Hunga Ha'apai hydration of the stratosphere. *Geophysical Research Letters*, *49*(13), e2022GL099381. https://doi.org/10.1029/2022GL099381

Mills, M. J., Richter, J. H., Tilmes, S., Kravitz, B., MacMartin, D. G., Glanville, A. A., et al. (2017). Radiative and chemical response to interactive stratospheric sulfate aerosols in fully coupled CESM1 (WACCM). *Journal of Geophysical Research: Atmospheres*, *122*(23), 13–061. https://doi.org/10.1002/2017JD027006

Mills, M. J., Schmidt, A., Easter, R., Solomon, S., Kinnison, D. E., Ghan, S. J., et al. (2016). Global volcanic aerosol properties derived from emissions, 1990–2014, using CESM1 (WACCM). *Journal of Geophysical Research: Atmospheres*, *121*(5), 2332–2348. https://doi.org/10.1002/2015JD024290

Proffitt, M. H., Margitan, J. J., Kelly, K. K., Loewenstein, M., Podolske, J. R., & Chan, K. R. (1990). Ozone loss in the Arctic polar vortex inferred from high-altitude aircraft measurements. *Nature*, *347*(6288), 31–36. https://doi.org/10.1038/347031a0

Santee, M. L., Lambert, A., Froidevaux, L., Manney, G. L., Schwartz, M. J., Millán, L. F., et al. (2023). Strong evidence of heterogeneous processing on stratospheric sulfate aerosol in the extrapolar Southern Hemisphere following the 2022 Hunga Tonga-Hunga Ha'apai eruption. *Journal of Geophysical Research: Atmospheres*, *128*(16), e2023JD039169. https://doi.org/10.1029/2023JD039169

Sellitto, P., Siddans, R., Belhadji, R., Carboni, E., Legras, B., Podglajen, A., & Kerridge, B. (2023). Observing the SO2 and sulphate aerosol plumes from the 2022 Hunga Tonga-Hunga Ha'apai eruption with IASI. *Authorea Preprints*.

Shi, Q., Jayne, J. T., Kolb, C. E., Worsnop, D. R., & Davidovits, P. (2001). Kinetic model for reaction of ClONO2 with H2O and HCl and HOCl with HCl in sulfuric acid solutions. *Journal of Geophysical Research*, *106*(D20), 24259–24274. https://doi.org/10.1029/2000jd000181

Slusser, J. R., Fish, D. J., Strong, E. K., Jones, R. L., Roscoe, H. K., & Sarkissian, A. (1997). Five years of NO2 vertical column measurements at Faraday (65 S): Evidence for the hydrolysis of BrONO2 on Pinatubo aerosols. *Journal of Geophysical Research*, *102*(D11), 12987–12993. https://doi.org/10.1029/97jd00359

Solomon, S. (1999). Stratospheric ozone depletion: A review of concepts and history. *Reviews of Geophysics*, *37*(3), 275–316. https://doi.org/10.1029/1999RG900008

Solomon, S., Dube, K., Stone, K., Yu, P., Kinnison, D., Toon, O. B., et al. (2022). On the stratospheric chemistry of midlatitude wildfire smoke. *Proceedings of the National Academy of Sciences*, *119*(10), e2117325119. https://doi.org/10.1073/pnas.2117325119

Solomon, S., Kinnison, D., Bandoro, J., & Garcia, R. (2015). Simulation of polar ozone depletion: An update. *Journal of Geophysical Research: Atmospheres*, *120*(15), 7958–7974. https://doi.org/10.1002/2015JD023365

Solomon, S., Stone, K., Yu, P., Murphy, D. M., Kinnison, D., Ravishankara, A. R., & Wang, P. (2023). Chlorine activation and enhanced ozone depletion induced by wildfire aerosol. *Nature*, *615*(7951), 259–264. https://doi.org/10.1038/s41586-022-05683-0

Stone, K. A., Solomon, S., Kinnison, D. E., Pitts, M. C., Poole, L. R., Mills, M. J., et al. (2017). Observing the impact of Calbuco volcanic aerosols on South Polar ozone depletion in 2015. *Journal of Geophysical Research: Atmospheres*, *122*(21), 11–862. https://doi.org/10.1002/2017JD026987

Strahan, S. E., Smale, D., Solomon, S., Taha, G., Damon, M. R., Steenrod, S. D., et al. (2022). Unexpected repartitioning of stratospheric inorganic chlorine after the 2020 Australian wildfires. *Geophysical Research Letters*, *49*(14), e2022GL098290. https://doi.org/10.1029/2022gl098290

Taha, G., Loughman, R., Colarco, P. R., Zhu, T., Thomason, L. W., & Jaross, G. (2022). Tracking the 2022 Hunga Tonga-Hunga Ha'apai aerosol cloud in the upper and middle stratosphere using space-based observations. *Geophysical Research Letters*, *49*(19), e2022GL100091. https://doi.org/10.1029/2022GL100091

Tie, X., & Brasseur, G. (1996). The importance of heterogeneous bromine chemistry in the lower stratosphere. *Geophysical Research Letters*, *23*(18), 2505–2508. https://doi.org/10.1029/96gl02121

Wang, P., Solomon, S., & Stone, K. (2023a). Stratospheric chlorine processing after the 2020 Australian wildfires derived from satellite data. *Proceedings of the National Academy of Sciences*, *120*(11), e2213910120. https://doi.org/10.1073/pnas.2213910120

Wang, X., Randel, W., Zhu, Y., Tilmes, S., Starr, J., Yu, W., et al. (2023b). Stratospheric climate anomalies and ozone loss caused by the Hunga Tonga-Hunga ha'apai volcanic eruption. *Journal of Geophysical Research: Atmospheres*, *128*(22), e2023JD039480. https://doi.org/10.1029/2023JD039480

Waschewsky, G. C., & Abbatt, J. P. (1999). HOBr in sulfuric acid solutions: Solubility and reaction with HCl as a function of temperature and concentration. *The Journal of Physical Chemistry A*, *103*(27), 5312–5320. https://doi.org/10.1021/jp984489i

Wilmouth, D. M., Østerstrøm, F. F., Smith, J. B., Anderson, J. G., & Salawitch, R. J. (2023). Impact of the Hunga Tonga volcanic eruption on stratospheric composition. *Proceedings of the National Academy of Sciences*, *120*(46), e2301994120. https://doi.org/10.1073/pnas.2301994120

Zambri, B., Solomon, S., Kinnison, D. E., Mills, M. J., Schmidt, A., Neely, R. R., et al. (2019). Modeled and observed volcanic aerosol control on stratospheric NOy and Cly. *Journal of Geophysical Research: Atmospheres*, *124*(17–18), 10283–10303. https://doi.org/10.1029/2019JD031111

Zhang, J., Kinnison, D., Zhu, Y., Wang, X., Tilmes, S., Dube, K., & Randel, W. (2024). Chemistry contribution to stratospheric ozone depletion after the unprecedented water-rich Hunga Tonga eruption. *Geophysical Research Letters*, *51*(7), e2023GL105762. https://doi.org/10.1029/2023GL105762

Zhang, J., Wang, P., Kinnison, D., Solomon, S., Guan, J., & Zhu, Y. (2024). Stratospheric chlorine processing after the unprecedented Hunga Tonga eruption. (Version 1.0.). [Dataset]. *UCAR/NCAR - GDEX*. https://doi.org/10.5065/j6yg-a009

Zhu, Y., Bardeen, C. G., Tilmes, S., Mills, M. J., Wang, X., Harvey, V. L., et al. (2022). Perturbations in stratospheric aerosol evolution due to the water-rich plume of the 2022 Hunga-Tonga eruption. *Communications Earth & Environment*, *3*(1), 248. https://doi.org/10.1038/s43247-022-00580-w

Zhu, Y., Portmann, R. W., Kinnison, D., Toon, O. B., Millán, L., Zhang, J., et al. (2023). Stratospheric ozone depletion inside the volcanic plume shortly after the 2022 Hunga Tonga eruption. *Atmospheric Chemistry and Physics*, *23*(20), 13355–13367. https://doi.org/10.5194/acp-23-13355-2023